X-ray structure and mechanism of RNA polymerase II stalled at an antineoplastic monofunctional platinum-DNA adduct

Dong Wang[a,b,1], Guangyu Zhu[c], Xuhui Huang[d], and Stephen J. Lippard[c,1]

[a]Department of Structural Biology, Stanford University School of Medicine, Stanford, CA 94305; [b]Skaggs School of Pharmacy and Pharmaceutical Sciences, University of California, San Diego, La Jolla, CA 92093; [c]Department of Chemistry, Massachusetts Institute of Technology, Cambridge, MA 02139; and [d]Department of Chemistry, Hong Kong University of Science and Technology, Clear Water Bay, Kowloon, Hong Kong, P.R. China

Contributed by Stephen J. Lippard, March 3, 2010 (sent for review February 9, 2010)

DNA is a major target of anticancer drugs. The resulting adducts interfere with key cellular processes, such as transcription, to trigger downstream events responsible for drug activity. *cis*-Diammine(pyridine)chloroplatinum(II), cDPCP or pyriplatin, is a monofunctional platinum(II) analogue of the widely used anticancer drug cisplatin having significant anticancer properties with a different spectrum of activity. Its novel structure-activity properties hold promise for overcoming drug resistance and improving the spectrum of treatable cancers over those responsive to cisplatin. However, the detailed molecular mechanism by which cells process DNA modified by pyriplatin and related monofunctional complexes is not at all understood. Here we report the structure of a transcribing RNA polymerase II (pol II) complex stalled at a site-specific monofunctional pyriplatin-DNA adduct in the active site. The results reveal a molecular mechanism of pol II transcription inhibition and drug action that is dramatically different from transcription inhibition by cisplatin and UV-induced 1,2-intrastrand cross-links. Our findings provide insight into structure-activity relationships that may apply to the entire family of monofunctional DNA-damaging agents and pave the way for rational improvement of monofunctional platinum anticancer drugs.

anticancer | chemotherapy | DNA damage | pyriplatin | transcription

The DNA template for transcription is not only the site of inborn errors of metabolism and of continuous attack by harmful environmental agents, but it also represents a major target for cancer therapy. Platinum-based anticancer drugs such as cisplatin, *cis*-diamminedichloroplatinum(II), are widely used and among the most effective antineoplastic treatments (1, 2). Platinum-based drugs typically form bifunctional intra- or interstrand DNA cross-links by covalent bonding to the N^7 positions of two guanosine residues, triggering a variety of cellular processes, including transcription inhibition with attendant apoptosis (1, 2). However, resistance and side effects can require withdrawal of these drugs before they can effect a cure in certain types of cancer (3).

In the effort to find new compounds that circumvent resistance to conventional bifunctional platinum-based drugs, a class of monofunctional platinum compounds were synthesized and screened for anticancer activity (4–6). In contrast to other inactive monofunctional platinum(II) compounds such as $[Pt(dien)Cl]^+$ and $[Pt(NH_3)_3Cl]^+$, *cis*-diammine(pyridine)chloroplatinum(II) [cDPCP or "pyriplatin" (Fig. 1)] and related complexes display significant anticancer properties and a different spectrum of activity compared to conventional platinum-based drugs. These features render them attractive candidates for treating cisplatin-refractory patients if the potency could be raised to or beyond the level of that of cisplatin (4, 5, 7). Pyriplatin exhibits unique chemical and biological properties, forming monofunctional DNA adducts (Fig. 1 and Fig. S1) that can inhibit transcription and better elude DNA repair (7). The x-ray crystal structure of pyriplatin bound to a DNA duplex reveals substantially different features than those of DNA adducts formed by conventional, bifunctional platinum-based drugs. The overall DNA duplex is much less distorted, with the pyridine ligand of the *cis*-$\{Pt(NH_3)_2(py)\}^{2+}$ moiety directed toward the 5′-end of the platinated strand. A hydrogen bond forms between the NH_3 ligand trans to pyridine and O^6 of the platinated guanosine residue (7).

The detailed molecular mechanism by which cells process DNA modified by monofunctional complexes such as pyriplatin is not understood. Several important questions remain unanswered. By what process do monofunctional adducts block pol II transcription? Does the mechanism differ from that of transcription inhibition by 1,2- and 1,3-intrastrand cross-links that comprise the major adducts of cisplatin? Why do pyriplatin and its homologues, which violate the classical structure-activity relationships (SARs) for active, bifunctional platinum drugs (8), show such promise by comparison to related monofunctional complexes like $[Pt(NH_3)_3Cl]^+$? Would knowledge of the structure of pyriplatin-modified DNA at its site(s) of biological action inform the design of more potent analogues?

In the present work we take a combined biochemical and x-ray structural approach to investigate the molecular mechanism of pol II transcription inhibition by a site-specific monofunctional platinum(II)-DNA adduct of pyriplatin. An unprecedented molecular mechanism for pol II transcription inhibition is revealed, providing insight into structure-activity relationships that may apply to the entire family of monofunctional DNA-damaging agents, whether or not they contain platinum.

Results

A Different Configuration of a Pyriplatin-DNA Adduct Accommodated in the Pol II Active Site. To understand how a monofunctional pyriplatin-DNA adduct is accommodated in the active site of the transcribing pol II elongation complex, we designed and prepared a DNA template containing a site-specific DNA lesion of this complex, as described previously (7). A transcribing pol II complex was then assembled in which the pyriplatin-DNA lesion occupies the active (+1) site (Complex B, Table 1). The crystal structure of this complex reveals that the platinated nucleotide is captured as a pol II complex in the post-translocation state, in which the addition site is empty and ready for NTP loading (*Dashed Ring*, Fig. 2*A* and Fig. S2). Fig. 2*A* reveals that the

Author contributions: D.W. and S.J.L. designed research; D.W., G.Z., and X.H. performed research; D.W., G.Z., X.H., and S.J.L. analyzed data; and D.W., X.H., and S.J.L. wrote the paper.

The authors declare no conflict of interest.

Data deposition: The atomic coordinates have been deposited in the Protein Data Bank, www.pdb.org (PDB ID codes 3M4O and 3M3Y).

[1]To whom correspondence may be addressed. E-mail: dongwang@ucsd.edu or lippard@mit.edu.

This article contains supporting information online at www.pnas.org/cgi/content/full/1002565107/DCSupplemental.

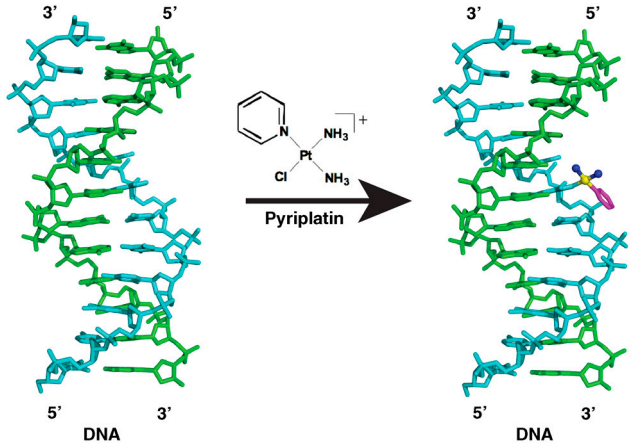

Fig. 1. Scheme depicting the formation of a monofunctional platinum-DNA adduct by pyriplatin on double-stranded duplex DNA. The structure of the pyriplatin-damaged DNA duplex used coordinates from the PDB (code 3CO3). The damaged and nondamaged DNA strands are shown in cyan and green, respectively. The pyridine ligand and two ammine groups of the *cis*-$\{Pt(NH_3)_2(py)\}^{2+}$ moiety are depicted in magenta and blue, respectively. The platinum atom and nitrogen atoms of the *cis*-$\{Pt(NH_3)_2(py)\}^{2+}$ moiety are highlighted in yellow and as a blue ball, respectively. The termini of the DNA strands are labeled.

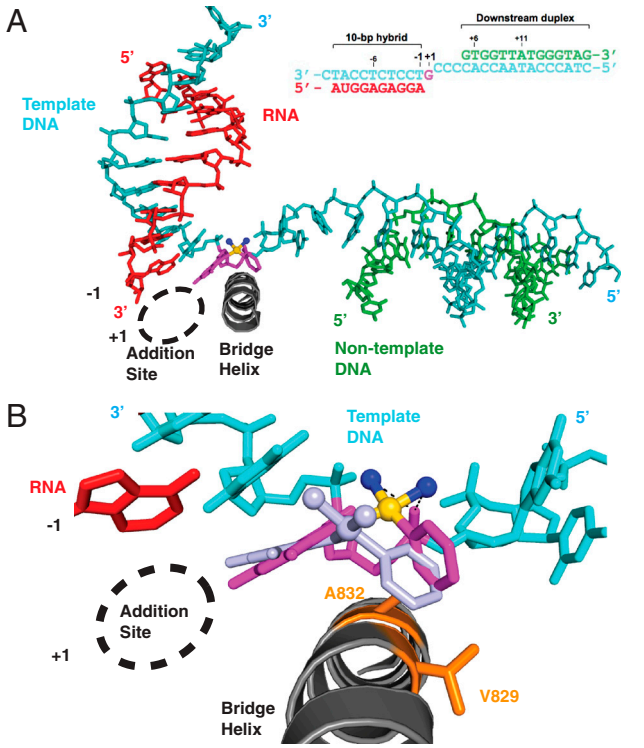

Fig. 2. Structure of a pol II transcribing complex encountering a site-specific pyriplatin-dG adduct in DNA. (*A*) A site-specific pyriplatin-DNA adduct is accommodated in the pol II active site. The view is a standard one, from the "Rpb2 side," as described elsewhere (9–11, 39). The RNA transcript, template DNA strand, and nontemplate DNA strand are depicted in red, cyan, and green, respectively. Parts of the bridge helix (Rpb1 825–848) are shown in gray. The pyriplatin-damaged guanosine is colored magenta. The platinum atom of the *cis*-$\{Pt(NH_3)_2(py)\}^{2+}$ moiety is denoted as a yellow ball and the two ammine groups are in blue. The dashed oval represents the empty nucleotide addition site in the post-translocation state. The positions of the RNA strand are labeled. (*B*) *cis*-$\{Pt(NH_3)_2(py)\}^{2+}$-dG in the pol II active site adopts a different configuration in comparison with its conformation in the structure of pyriplatin-modified duplex DNA. The superimposed geometry of the *cis*-$\{Pt(NH_3)_2(py)\}^{2+}$-guanosine unit from the DNA duplex structure (3CO3) is shown in light blue. Side chains of Val 829 and Ala 832 are depicted in orange. The remainder of the figure is the same as in *A*.

positioning of the pyriplatin-damaged guanosine residue is located above the bridge helix. This structure requires rotation of the *cis*-$\{Pt(NH_3)_2(py)\}^{2+}$ moiety and its bound guanosine residue into a different configuration compared to that adopted in the pyriplatin-duplex DNA structure, in order to avoid a steric clash with bridge helix (7). Fig. 2*B* depicts this comparison. The rotation is energetically facilitated by the formation of hydrogen bonds between the ammine ligands on platinum with the phosphodiester moiety of the backbone between positions +1 and +2, with concomitant loss of a hydrogen bond between O^6 of the platinated guanosine residue and an ammine ligand. An additional feature is that the pyridine group of the *cis*-$\{Pt(NH_3)_2(py)\}^{2+}$ fragment, which points downstream toward the 5′-direction of the template DNA, forms van der Waals interactions with bridge helix residues Val 829 and Ala 832. The purine base of the guanosine residue at position +1 is displaced toward the major groove of the RNA–DNA duplex by comparison with structures having an undamaged base at this site in the post-translocation state (9–11).

Transcription Elongation Inhibited by a Pyriplatin–DNA Adduct. Because transcription inhibition is an important component in the mechanism of action of platinum anticancer drugs (12–20), we investigated the effect of a site-specific pyriplatin–DNA adduct on the kinetics of pol II transcription elongation. We performed an extension assay using platinated (Complex A, Table 1) and unplatinated (Complex A′, control, Table 1) pol II transcribing complexes having a 9mer RNA as primer. These complexes were then incubated with a mixture of ATP, CTP, and GTP. The RNA transcripts in A could be elongated from the 9mer to the 11mer, stopping at a position corresponding to the Pt–DNA lesion site observed in the pol II complex of the damaged template DNA, whereas RNA transcripts in A′ were extended much farther downstream on the undamaged template control DNA (Fig. 3*A*). In order to avoid the possibility of misincorporation-induced transcription inhibition in this assay, we carried out a similar extension assay using an RNA containing a 3′-end CMP matched against the damaged base (pol II complex C, 11mer) (Table 1). A single matching GTP was incubated with this pol II complex to test whether the enzyme could bypass the Pt–DNA lesion. Consistent with the results of the previous assay, RNA transcripts could not be extended beyond an 11mer in the pol II complex with the damaged DNA template, whereas RNA transcripts were efficiently extended farther downstream along the undamaged DNA template (Fig. 3*B*). Similar extension assay results were obtained using a chain-terminated GTP analogue 3′-dGTP or an RNA primer of different length (complex B, 10mer) (Table 1) (Fig. 3 *C* and *D*). Finally, to investigate whether the presence of the damaged base affects the rate of NTP incorporation in a single round, we used complex B (10mer) and complex C (11mer), incubating with CTP and 3′-dGTP, respectively. For CTP incorporation, RNA transcripts could be efficiently extended from the 10mer to the 11mer using both damaged and nondamaged templates at a comparable rate (Fig. 3*E*), whereas no obvious extension of RNA transcripts from the 11mer to a 12mer was observed on the damaged DNA template (Fig. 3*C*). UTP failed to incorporate at the damaged template under the same conditions (Fig. S3*A*). No obvious intrinsic cleavage was observed for a pol II complex containing the 11mer RNA and Pt-damaged DNA template in the presence of 20 mM Mg^{2+} ion, suggesting that most of complex C (11mer) is not in the backtracked state (Fig. S3*B*) (21–23).

X-ray Structure of Pol II stalled at a Pyriplatin–DNA Adduct. To understand the nature of the pol II complex stalled at the pyriplatin-induced Pt–DNA adduct, we solved the x-ray crystal structure

BIOCHEMISTRY

Table 1. RNA and DNA scaffold of pol II transcribing complexes

Complex A: (Damaged template 29mer with 9mer RNA)

```
RNA: 5′  AUGGAGAGG  3′
DNA: 3′ CTACCTCTCCTG*CCCCACCAATACCCATC  5′
DNA: 5′                GTGGTTATGGGTAG  3′
```

Complex A′: (Nondamaged template 29mer with 9mer RNA)

```
RNA: 5′  AUGGAGAGG  3′
DNA: 3′ CTACCTCTCCTGCCCCACCAATACCCATC  5′
DNA: 5′                GTGGTTATGGGTAG  3′
```

Complex B: (Damaged template 29mer with 10mer RNA)

```
RNA: 5′  AUGGAGAGGA 3′
DNA: 3′ CTACCTCTCCTG*CCCCACCAATACCCATC  5′
DNA: 5′                GTGGTTATGGGTAG  3′
```

Complex B′: (Nondamaged template 29mer with 10mer RNA)

```
RNA: 5′  AUGGAGAGGA 3′
DNA: 3′ CTACCTCTCCTGCCCCACCAATACCCATC  5′
DNA: 5′                GTGGTTATGGGTAG  3′
```

Complex C: (Damaged template 29mer with 11mer RNA)

```
RNA: 5′  AUGGAGAGGAC3′
DNA: 3′ CTACCTCTCCTG*CCCCACCAATACCCATC  5′
DNA: 5′                GTGGTTATGGGTAG  3′
```

Complex C′: (Non-damaged Template 29mer with 11mer RNA)

```
RNA: 5′  AUGGAGAGGAC3′
DNA: 3′ CTACCTCTCCTGCCCCACCAATACCCATC  5′
DNA: 5′                GTGGTTATGGGTAG  3′
```

G*: cDPCP-dG.

of the enzyme in complex with a platinated DNA using an RNA-containing CTP matched against the damaged guanosine residue. In this structure, pol II is in pre-translocation state, with the newly added CMP still occupying the addition site without translocation. The platinated guanosine residue forms Watson–Crick base pairs with the newly added CMP (Fig. 4 *A* and *B* and Fig. S4). The *cis*-$\{Pt(NH_3)_2(py)\}^{2+}$ moiety is surrounded by the bridge helix at the bottom, part of the Rpb2 fork region (528–534) on the left side, and the sugar-phosphate backbone connecting template DNA positions +1 and +2 on the right side (Fig. 4*B*). Interestingly, upon CMP incorporation, the *cis*-$\{Pt(NH_3)_2(py)\}^{2+}$ moiety adopts a different conformation. The pyridine group of this unit now faces toward 3′-direction of template DNA (Fig. 4 *A* and *B*). The ammine group trans to pyridine is directed toward the bridge helix and forms hydrogen bonds with main chain atoms of Ala 828 and the side chain of Thr 831 (Fig. 4*B*). The residues in the bridge helix are highly conserved from yeast to humans. Because Thr 831 and Ala 828 are absolutely conserved between *S. cerevisiae* and humans, the interactions we observe in the *S. cerevisiae* pol II structure will also occur in human pol II.

These structural results provide important insights into the transcription stalling process at a monofunctional pyriplatin–DNA adduct. The adduct adopts a significantly different conformation within the pol II active site compared to that in duplex DNA (7). The present structural and biochemical evidence reveals that pol II stalls after efficient incorporation of CTP against the damaged guanosine residue. The conformation of the pyriplatin–DNA adduct changes significantly upon incorporation of CTP. The modified guanosine rotates into the pol II active site and serves as a template for base pairing with the matched substrate, and the *cis*-$\{Pt(NH_3)_2(py)\}^{2+}$ moiety is now directed toward 3′-end of the platinated DNA.

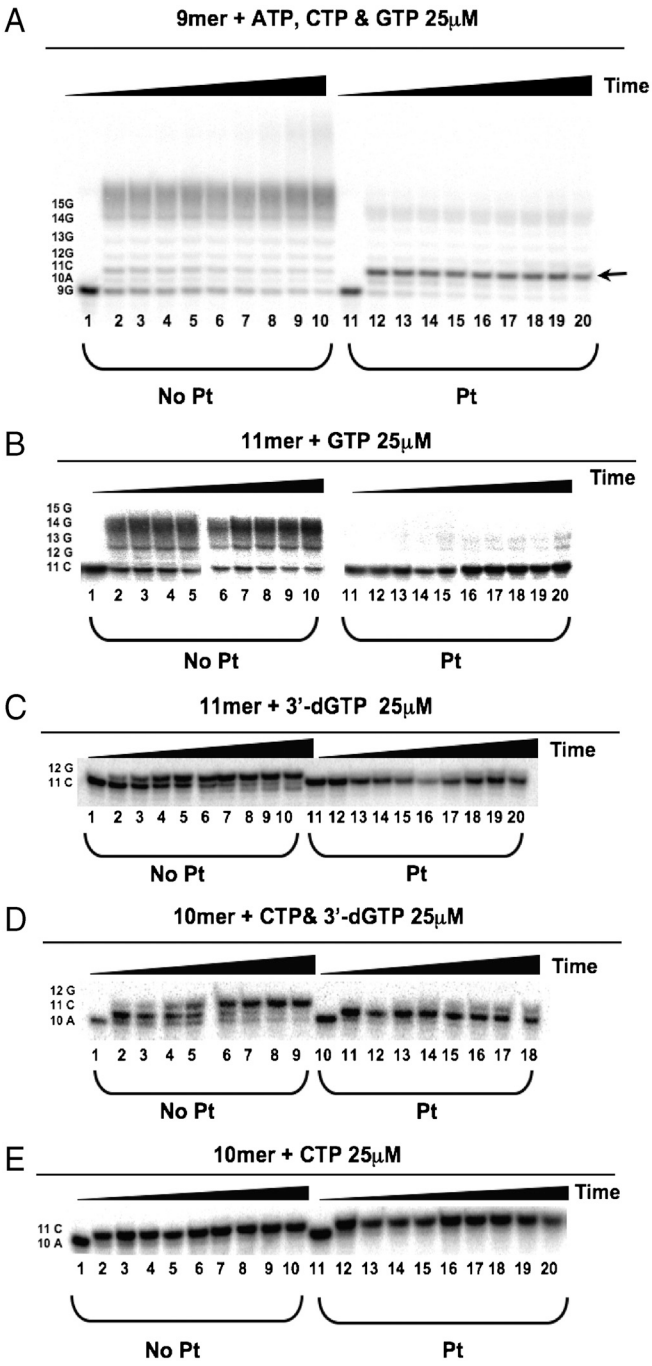

Fig. 3. Pol II transcription elongation blocked by a site-specific pyriplatin-DNA adduct. (*A*) In vitro transcription with preformed pol II elongation complexes A and A′ incubated with a mixture of ATP, CTP, and GTP (25 μM each). Time points were taken after 0, 0.5, 1, 2, 3, 4, 8, 16, 32, or 64 min incubation. The RNA transcripts in lanes 1–10 were taken from reactions of the pol II complex with a nondamaged DNA template, whereas the RNA transcripts in lanes 11–20 were taken from reactions of the pol II complex with a site-specifically damaged DNA template. The stalled RNA transcript is indicated by a black arrow (*Right*), and the extended RNA transcript is visible to the left. The length and sequences of RNA transcripts are given at the left margin of the gel. (*B*) In vitro transcription with preformed pol II elongation complexes C and C′ incubated with 25 μM GTP. The remainder of gel is the same as in *A*. (*C*) In vitro transcription with preformed pol II elongation complexes C and C′ incubated with 25 μM of 3′-dGTP. The rest of gel is same as in *A*. (*D*) In vitro transcription with preformed pol II elongation complexes B and B′ incubated with a mixture of 25 μM CTP and 3′-dGTP. Time points were taken after 0, 0.5, 1, 2, 4, 8, 16, 32, 64 min of incubation. The rest of gel is the same as in *A*. (*E*) In vitro transcription with preformed pol II elongation complexes B and B′ incubated with 25 μM CTP. The remainder of the gel is the same as in *A*.

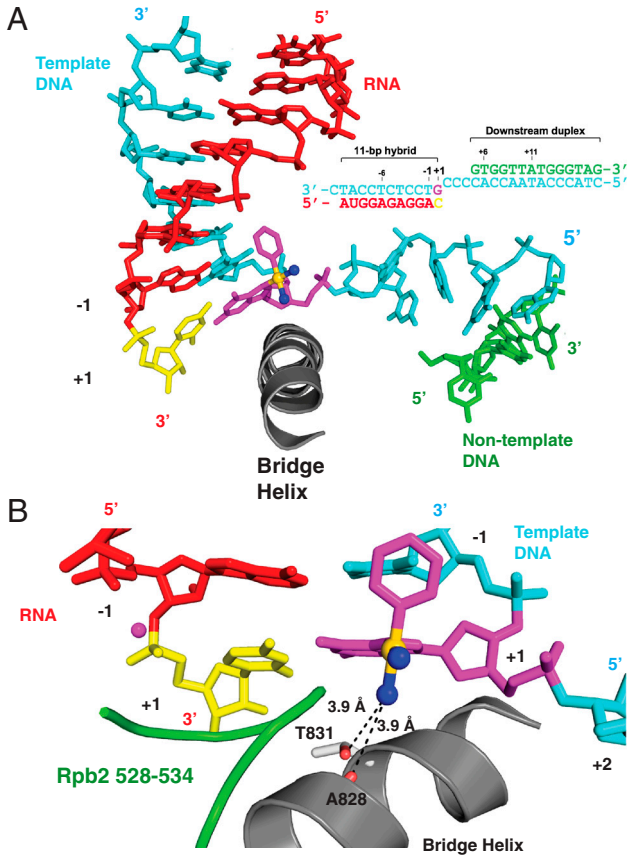

Fig. 4. Structure of pol II transcribing complex stalled at a site-specific pyriplatin-DNA adduct after CMP incorporation. (*A*) The newly incorporated matched CMP is highlighted in yellow. Other colors are as in Fig. 2. Interactions of the damaged nucleotide and pol II residues are highlighted in (*B*). The view is taken roughly from an ~90 degree clockwise rotation along the RNA/DNA helix axis from *A*. Nitrogen and oxygen atoms are depicted in blue and red, respectively. Hydrogen bonds between ammine group of the *cis*-$\{Pt(NH_3)_2(py)\}^{2+}$ moiety and bridge helix residues are shown as black dashed lines. The loop of Rpb2 828–834 is shown in green.

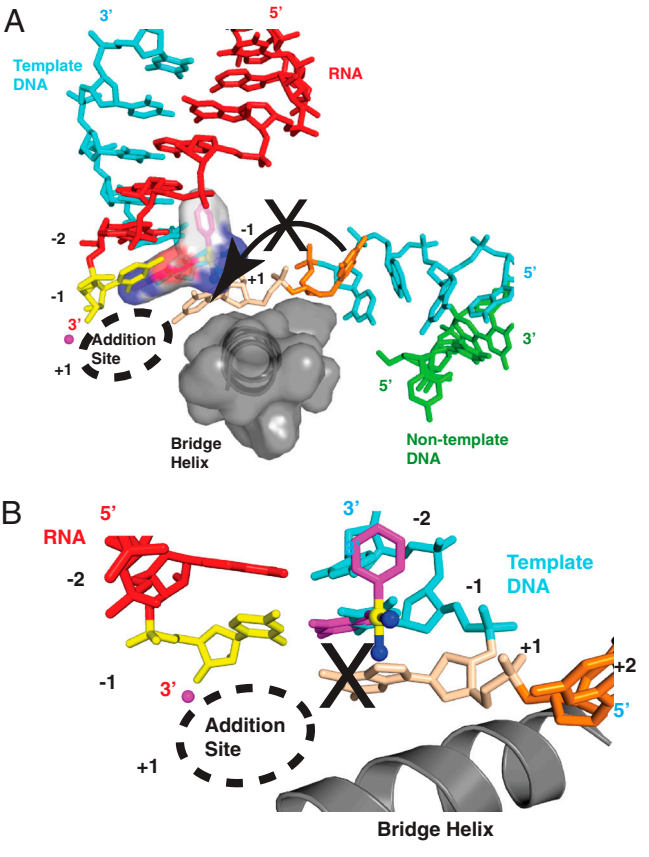

Fig. 5. Pol II translocation following CMP incorporation is inhibited by a site-specific pyriplatin-DNA adduct. (*A*) The *cis*-$\{Pt(NH_3)_2(py)\}^{2+}$-guanosine unit is superimposed with a nucleoside in −1 position shown in magenta and as a surface view. In the latter, the nitrogen and oxygen atoms are highlighted in blue and red, respectively. CMP at the 3′-end of RNA chain is highlighted in yellow. The bridge helix is shown in gray as a surface view. The nucleosides at the +1 and +2 position of the template DNA are drawn in wheat and orange, respectively. The rotation of the downstream nucleoside base during translocation, from the +2 position to the +1 position, is blocked by the *cis*-$\{Pt(NH_3)_2(py)\}^{2+}$ moiety, as indicated. Other colors are as in Fig. 2. (*B*) The *cis*-$\{Pt(NH_3)_2(py)\}^{2+}$ moiety of pyriplatin-dG adduct modeled at −1 position clashes with the base at the +1 position. Colors are as in *A*, and the view as in Fig. 4*B*.

The result is that the RNA transcript fails to extend beyond the site of damage, subsequent translocation and nucleotide addition being strongly inhibited. Several factors contribute to such translocation inhibition, including (*i*) stabilization of the initial pre-translocation state by interaction between the platinated guanosine and pol II residues (Fig. 4*B*); (*ii*) a high translocation energy barrier; and (*iii*) an unfavorable subsequent post-translocation state induced by the DNA lesion. Hydrogen bonding interactions between an ammine group of the *cis*-$\{Pt(NH_3)_2(py)\}^{2+}$ moiety with bridge helix partially help to stabilize the initial pre-translocation state (Fig. 4*B*). To address the factors *ii* and *iii*, we modeled the pyriplatin-damaged guanosine residue at the −1 position to mimic the state following translocation of the pyriplatin-modified guanosine from the +1 to −1 position. The structure clearly reveals that the *cis*-$\{Pt(NH_3)_2(py)\}^{2+}$ moiety serves as a strong steric block, narrowing the space between the DNA nucleotide base (−1) and the bridge helix and preventing the downstream undamaged nucleoside base on the DNA template strand from rotating into the canonical +1 position (Fig. 5*A*). Moreover, the fact that the *cis*-$\{Pt(NH_3)_2(py)\}^{2+}$ moiety at the −1 position sterically clashes with the downstream nucleotide base at the +1 position suggests that this final state is unfavorable (Fig. 5 *A* and *B*). In summary, our results indicate that pyriplatin–DNA adducts inhibit pol II transcription elongation by preventing subsequent translocation and nucleotide addition beyond the site of damage.

Discussion

Insights into Structure-Activity Relationships (SARs) for the Monofunctional Platinum Drug Family. The original SARs pertaining to bifunctional platinum compounds such as cisplatin (8) were formulated to explain why anticancer activity appeared to require neutral, *cis*-$[PtA_2X_2]$ compositions, in which A is an amine ligand and X is a monoanionic leaving group. These rules are clearly violated by cationic, monofunctional platinum compounds such as pyriplatin (4, 5). Other monofunctional platinum complexes, including $[Pt(dien)Cl]^+$, $[Pt(NH_3)_3Cl]^+$, and *trans*-$[Pt(NH_3)_2(py)Cl]^+$, are inactive and do not arrest pol II transcription, whereas the *cis*-$\{Pt(NH_3)_2(py)\}^{2+}$ unit bound to guanosine blocks pol II transcription and has significant anticancer properties in mice when administered as pyriplatin (4, 5, 8, 24–32).

The present structure of pol II in complex with DNA site-specifically modified by pyriplatin provides unique insight into SARs to be expected for monofunctional platinum drug candidates. We constructed models of potential stalled transcription complexes containing DNA modified by the following three representative units, $\{Pt(NH_3)_3\}^{2+}$, *trans*-$\{Pt(NH_3)_2(py)\}^{2+}$, and *cis*-$\{Pt(NH_3)_2(py)\}^{2+}$ bound to guanosine in DNA and positioned in either the −1 or +1 site of pol II, in order to mimic the

post- and pre-translocation states, respectively (Fig. S1). For each modeled structure, we rotated the platinum unit about the Pt-N^7 bond by 360° and computed van der Waals energies arising from contacts between platinum ligands and the rest of the pol II complex (Figs. S5–S9). The $\{Pt(NH_3)_3\}^{2+}$ and *trans*-$\{Pt(NH_3)_2(py)\}^{2+}$ moieties could be readily accommodated within the pol II active site over wide energy minima. The lack of a significant steric clash for these two groups, in either the −1 or +1 position of the pol II transcribing complex, indicates the absence of a barrier to transcriptional bypass (Figs. S6–S9). This finding agrees with experiment. In contrast, the energy barrier is prohibitively high for *cis*-$\{Pt(NH_3)_2(py)\}^{2+}$ platinated DNA modeled at −1 position, which is consistent with its ability to block pol II bypass and the failure of pol II to reach the subsequent post-translocation state (Figs. S5 and S8). The presence of a pyridine or other bulky group in the cis configuration is important for restricting the rotation range of the *cis*-$\{Pt(NH_3)_2(py)\}^{2+}$ moiety and thus rendering it a strong steric block to translocation. For a $\{Pt(NH_3)_3\}^{2+}$ or *trans*-$\{Pt(NH_3)_2(py)\}^{2+}$ adduct at the −1 position, such a steric clash can be avoided by rotation about the Pt-N^7 bond, facilitating subsequent pol II translocation. These results are fully consistent with previous biochemical studies revealing that the latter two DNA adducts are inactive and fail to block transcription (5, 7, 12, 26–33).

A Unique Molecular Mechanism of Pol II Transcription Inhibition. The stalling mechanism of monofunctional platinum drugs of the pyriplatin family is dramatically different from transcription inhibition by cisplatin and UV-induced 1,2-intrastrand cross-links. For the latter two DNA-modifications, a translocation barrier prevents delivery of damaged bases to the active site and/or leads to misincorporation of NTPs against the damage site, respectively (19, 34). Monofunctional platinum-damaged residues, on the other hand, can cross over the bridge helix and be accommodated in the pol II active site. For Pt–dG adducts, the correct CMP nucleotide can be efficiently incorporated against the damaged guanosine. It is blockage of the subsequent translocation from this position after incorporation of the cytosine nucleotide that leads to inhibition of the RNA polymerase, but only when a bulky pyridine ligand is present in the *cis* coordination site.

In conclusion, we report here the structure of a pol II transcribing complex stalled at a site-specific monofunctional DNA adduct, revealing a unique mechanism of transcription inhibition by this kind of genome damage. The results establish a basis for SARs that govern the anticancer drug potential of monofunctional platinum-based DNA-damaging agents. Specific interactions between pol II active site residues and the platinum ligands are revealed, providing a structural framework for rational design of more potent monofunctional pyriplatin analogues. Because the spectrum of activity of pyriplatin is dramatically different from that of cisplatin against an extensive panel of cancer cell lines but with reduced potency (7), this information will be valuable for increasing the anticancer drug potential of this family of compounds based on pol II stalling with concomitant induction of apoptosis.

Methods

Preparation of Pol II Transcribing Complexes. Ten-subunit *S. cerevisiae* pol II was purified as described (35). RNA oligonucleotides were purchased from Dharmacon and DNA oligonucleotides were obtained from IDT. *cis*-$[Pt(NH_3)_2(py)Cl]Cl$ was prepared by Ryan Todd at MIT. The site-specifically platinated template DNA was obtained as described (7).

Pol II transcribing complexes were assembled with the use of synthetic oligonucleotides (10). Briefly, DNA and RNA oligonucleotides were annealed and mixed with pol II in 20 mM Tris (pH 7.5), 40 mM KCl, and 5 mM DTT. The final mixture contained 2 μM pol II, 10 μM site-specific pyriplatin-damaged template DNA strand, and 20 μM nontemplate DNA and RNA oligonucleotides. The mixture was kept for 1 h at room temperature, and excess oligonucleotides were removed by ultrafiltration. Crystals were obtained from solutions containing 390 mM $(NH_4)_2HPO_4/NaH_2PO_4$, pH 5.9–6.3, 50 mM dioxane, 10 mM DTT, and 9–11% PEG6000. Crystals of transcribing complexes were transferred in a stepwise manner to cryobuffer as described (10, 11). For the structure of the pol II complex with CTP incorporation, 10 mM CTP was added to the cryobuffer (10, 11).

Crystal Structure Determination and Analysis. Diffraction data were collected on beam line 11-1 at the Stanford Synchrotron Radiation Laboratory. Data were processed in DENZO and SCALEPACK (HKL2000) (36). Model building was performed with the program Coot (37), and refinement was done with REFMAC with TLS (CCP4i) (Table S1). In the structure of pol II complex with a CTP incorporation against damaged guanosine residue, we also observed additional weaker density within the second channel in comparison to the nucleoside residue at the +1 position, which may correspond to nonspecific binding of a second CTP molecule through the soaking process. All structure models in the figures were superimposed with nucleoside residues near the active site using PYMOL (38).

Transcription Assay. Transcription assays were performed essentially as described (11). In a typical reaction, ^{32}P-labeled RNA oligonucleotide (10 pmol) was annealed with template DNA 29mer (20 pmol, damaged or nondamaged template) and nontemplate DNA 14mer (20 pmol) in elongation buffer (20 mM Tris-HCl, pH 7.5, 40 mM KCl, 0.5 mM $MgCl_2$) in a final volume of 20 μL. An aliquot of the annealed RNA/DNA hybrid was incubated with a five-fold excess of pol II (final concentration of pol II 1.1 μM, of RNA oligonucleotide 0.22 μM, and of DNA oligonucleotides 0.44 μM) for 10 min at room temperature. Equal volumes of the NTP mixture solution were added (final concentrations 25 μM) and the mixture was then incubated for 0, 0.5, 1, 2, 3, 4, 8, 16, 32, or 64 min at room temperature before addition of stop solution (final concentrations 5 M urea, 44.5 mM Tris-HCl, 44.5 mM boric acid, 26 mM EDTA, pH 8.0, Xylene Cyanol and Bromophenol Blue dyes). RNA products were analyzed by PAGE in the presence of urea. Visualization and quantification of products were performed with the use of a PhosphorImager (Molecular Dynamics).

Computer Modeling Analysis. Three representative platinum units, $\{Pt(NH_3)_3\}^{2+}$, *trans*-$\{Pt(NH_3)_2(py)\}^{2+}$, and *cis*-$\{Pt(NH_3)_2(py)\}^{2+}$ bound to guanosine in DNA and positioned in either the −1 or +1 site of pol II were modeled to mimic the post- and pre-translocation states, respectively. The vdW interaction energies between the three ligands at different orientations and the rest of the pol II complex were systematically computed and taken as direct indicators of steric effects.

The structure of the *cis*-$\{Pt(NH_3)_2(py)\}^{2+}$ fragment on DNA in pol II is available from the current study. Initial configurations for the other two units, $\{Pt(NH_3)_3\}^{2+}$ and *trans*-$\{Pt(NH_3)_2(py)\}^{2+}$, were obtained by modeling. Briefly, the same configuration of pol II, DNA, and RNA as found in the structure containing *cis*-$\{Pt(NH_3)_2(py)\}^{2+}$ was used for these two complexes. The geometry of the $\{Pt(NH_3)_3\}^{2+}$ moiety was taken from a previous structure where it binds to a B-DNA dodecamer (PDB ID: 5BNA) (39). Docking was achieved by aligning the damaged guanosine base of the two structures. Finally, the *trans*-ammine group in $\{Pt(NH_3)_3\}^{2+}$ was replaced with a pyridine ligand, and the Pt-N bond length was appropriately adjusted to obtain the structure for *trans*-$\{Pt(NH_3)_2(py)\}^{2+}$. The same procedure was used to generate structures at both +1 and −1 positions.

The vdW energies were computed for different configurations generated by rotating about the Pt-N^7 bond from −180° to 180° for each platinum modification (see Figs. S5–S7). The rotation angle (φ) was defined to be positive when rotating in the anticlockwise direction. In the configuration with $\varphi = 0°$, the plane composed of two Pt-N bonds of the ligand which are perpendicular to the Pt-N^7 bond was set to be parallel to the damaged guanosine base. We noticed that, for $\{Pt(NH_3)_3\}^{2+}$ and *trans*-$\{Pt(NH_3)_2(py)\}^{2+}$, two trans ammine groups were accommodated at slightly different configurations, with $\varphi = 0°$ due to the different local environment, which leads to slightly different energies between conformations with φ and $\varphi \pm 180°$. Because the purpose of our modeling study is to identify major steric clashes instead of accurately computing free energy changes associated with rotation of the ligand, which requires extensive conformational sampling, we performed a simple average of the two energies ($E_1(\varphi)$ and $E_2(\varphi \pm 180°)$) based on their Boltzmann weights (T 298 K), eq 1,

$$\tilde{E} = (e^{-\beta E_1}E_1 + e^{-\beta E_2}E_2)/(e^{-\beta E_1} + e^{-\beta E_2}) \quad [1]$$

to get a better estimate of vdW energy profiles.

The GROMACS simulation package was used to compute vdW energies between the ligands and the pol II complex (40). A 20-Å cutoff was adopted for computing the vdW interactions. The AMBER03 force field was used for the pol II complex including protein, RNA, and DNA (41). The vdW force field (Leonard–Jones potential) parameters for ligands were generated from the AMTECHAMBER module of the AMBER 9 package (42) using the general AMBER force field (GAFF) (43) developed for rational drug design. Since the Pt atom is not in direct contact with the pol II complex and does not contribute significantly to any steric effects, we excluded it from our vdW energy calculations.

ACKNOWLEDGMENTS. This research was supported by the National Institute of General Medical Sciences (NIH Pathway to Independence Award GM085136 to D.W. and GM49985 to R.D. Kornberg) and by the National Cancer Institute (Grant CA034992 to S.J.L.). Portions of the research were carried out at the Stanford Synchrotron Radiation Laboratory, a national user facility operated by Stanford University on behalf of the U.S. Department of Energy, Office of Basic Energy Sciences. The SSRL Structural Molecular Biology Program is supported by the Department of Energy, Office of Biological and Environmental Research, and by the National Institutes of Health, National Center for Research Resources, Biomedical Technology Program, and the National Institute of General Medical Sciences.

1. Jamieson ER, Lippard SJ (1999) Structure, recognition, and processing of cisplatin–DNA adducts. *Chem Rev* 99:2467–2498.
2. Wang D, Lippard SJ (2005) Cellular processing of platinum anticancer drugs. *Nat Rev Drug Discov* 4:307–320.
3. Roy S, et al. (2008) Phenanthroline derivatives with improved selectivity as DNA-targeting anticancer or antimicrobial drugs. *ChemMedChem* 3:1427–1434.
4. Hollis LS, Amundsen AR, Stern EW (1989) Chemical and biological properties of a new series of *cis*-diammineplatinum(II) antitumor agents containing three nitrogen donors: *cis*-$[Pt(NH_3)_2(\text{N-donor})Cl]^+$. *J Med Chem* 32:128–136.
5. Hollis LS, et al. (1991) Mechanistic studies of a novel class of trisubstituted platinum(II) antitumor agents. *Cancer Res* 51:1866–1875.
6. Bierbach U, Sabat M, Farrell N (2000) Inversion of the cis geometry requirement for cytotoxicity in structurally novel platinum(II) complexes containing the bidentate N,O-donor pyridin-2-yl-acetate. *Inorg Chem* 39:1882–1890.
7. Lovejoy KS, et al. (2008) *cis*-Diammine(pyridine)chloroplatinum(II), a monofunctional platinum(II) antitumor agent: Uptake, structure, function, and prospects. *Proc Natl Acad Sci USA* 105:8902–8907.
8. Cleare MJ, Hoeschele JD (1973) Studies on the antitumor activity of group VIII transition metal complexes. Part I. Platinum (II) complexes. *Bioinorg Chem* 2:187–210.
9. Westover KD, Bushnell DA, Kornberg RD (2004) Structural basis of transcription: separation of RNA from DNA by RNA polymerase II. *Science* 303:1014–1016.
10. Westover KD, Bushnell DA, Kornberg RD (2004) Structural basis of transcription: nucleotide selection by rotation in the RNA polymerase II active center. *Cell* 119:481–489.
11. Wang D, et al. (2006) Structural basis of transcription: Role of the trigger loop in substrate specificity and catalysis. *Cell* 127:941–954.
12. Corda Y, et al. (1993) Spectrum of DNA–platinum adduct recognition by prokaryotic and eukaryotic DNA-dependent RNA polymerases. *Biochemistry* 32:8582–8588.
13. Mello JA, Lippard SJ, Essigmann JM (1995) DNA adducts of *cis*-diamminedichloroplatinum(II) and its trans isomer inhibit RNA polymerase II differentially *in vivo*. *Biochemistry* 34:14783–14791.
14. Sandman KE, Marla SS, Zlokarnik G, Lippard SJ (1999) Rapid fluorescence-based reporter-gene assays to evaluate the cytotoxicity and antitumor drug potential of platinum complexes. *Chem Biol* 6:541–551.
15. Lee KB, Wang D, Lippard SJ, Sharp PA (2002) Transcription-coupled and DNA damage-dependent ubiquitination of RNA polymerase II *in vitro*. *Proc Natl Acad Sci USA* 99:4239–4244.
16. Tornaletti S, Patrick SM, Turchi JJ, Hanawalt PC (2003) Behavior of T7 RNA polymerase and mammalian RNA polymerase II at site-specific cisplatin adducts in the template DNA. *J Biol Chem* 278:35791–35797.
17. Tremeau-Bravard A, Riedl T, Egly JM, Dahmus ME (2004) Fate of RNA polymerase II stalled at a cisplatin lesion. *J Biol Chem* 279:7751–7759.
18. Jung Y, Lippard SJ (2006) RNA polymerase II blockage by cisplatin-damaged DNA. Stability and polyubiquitylation of stalled polymerase. *J Biol Chem* 281:1361–1370.
19. Damsma GE, et al. (2007) Mechanism of transcriptional stalling at cisplatin-damaged DNA. *Nat Struct Mol Biol* 14:1127–1133.
20. Jung Y, Lippard SJ (2007) Direct cellular responses to platinum-induced DNA damage. *Chem Rev* 107:1387–1407.
21. Surratt CK, Milan SC, Chamberlin MJ (1991) Spontaneous cleavage of RNA in ternary complexes of *Escherichia coli* RNA polymerase and its significance for the mechanism of transcription. *Proc Natl Acad Sci USA* 88:7983–7987.
22. Orlova M, et al. (1995) Intrinsic transcript cleavage activity of RNA polymerase. *Proc Natl Acad Sci USA* 92:4596–4600.
23. Wang D, et al. (2009) Structural basis of transcription: backtracked RNA polymerase II at 3.4 angstrom resolution. *Science* 324:1203–1206.
24. Cohen GL, Bauer WR, Barton JK, Lippard SJ (1979) Binding of *cis*- and *trans*-dichlorodiammineplatinum(II) to DNA: evidence for unwinding and shortening of the double helix. *Science* 203:1014–1016.
25. Lecointe P, Macquet JP, Butour JL (1979) Correlation between the toxicity of platinum drugs to L1210 leukemia cells and their mutagenic properties. *Biochem Biophys Res Commun* 90:209–213.
26. Macquet JP, Butour JL (1983) Platinum-amine compounds: importance of the labile and inert ligands for their pharmacological activities toward L1210 leukemia cells. *J Natl Cancer Inst* 70:899–905.
27. Calvert AH (1986) Clinical applications of platinum metal complexes. *Biochemical Mechanisms of Platinum Antitumor Drugs* (IRI Press, Washington).
28. Balcarová Z, et al. (1998) DNA interactions of a novel platinum drug, *cis*-$[PtCl(NH_3)_2(\text{N7-acyclovir})]^+$. *Mol Pharmacol* 53:846–855.
29. Brabec V, Leng M (1993) DNA interstrand cross-links of *trans*-diamminedichloroplatinum(II) are preferentially formed between guanine and complementary cytosine residues. *Proc Natl Acad Sci USA* 90:5345–5349.
30. Lemaire MA, Schwartz A, Rahmouni AR, Leng M (1991) Interstrand cross-links are preferentially formed at the d(GC) sites in the reaction between *cis*-diamminedichloroplatinum (II) and DNA. *Proc Natl Acad Sci USA* 88:1982–1985.
31. Brabec V, Boudny V (1994) Monofunctional and interstrand DNA adducts of platinum (II) complexes. *Met Based Drugs* 1:195–200.
32. Brabec V, Boudný V, Balcarová Z (1994) Monofunctional adducts of platinum(II) produce in DNA a sequence-dependent local denaturation. *Biochemistry* 33:1316–1322.
33. Novakova O, et al. (2009) Energetics, conformation, and recognition of DNA duplexes modified by methylated analogues of $[PtCl(\text{dien})]^+$. *Chemistry* 15:6211–6221.
34. Brueckner F, Hennecke U, Carell T, Cramer P (2007) CPD damage recognition by transcribing RNA polymerase II. *Science* 315:859–862.
35. Cramer P, Bushnell DA, Kornberg RD (2001) Structural basis of transcription: RNA polymerase II at 2.8 angstrom resolution. *Science* 292:1863–1876.
36. Otwinowski Z, Minor W (1997) Processing of x-ray diffraction data collected in oscillation mode. *Method Enzymol* 276:307–326.
37. Emsley P, Cowtan K (2004) Coot: Model-building tools for molecular graphics. *Acta Cryst* D60:2126–2132.
38. DeLano WL (2002) *The PyMOL Molecular Graphics System* (DeLano Scientific, Palo Alto, CA).
39. Wing RM, Pjura P, Drew HR, Dickerson RE (1984) The primary mode of binding of cisplatin to a B-DNA dodecamer: C-G-C-G-A-A-T-T-C-G-C-G. *EMBO J* 3:1201–1206.
40. Lindahl E, Hess B, van der Spoel D (2001) GROMACS 3.0: A package for molecular simulation and trajectory analysis. *J Mol Model* 7:306–317.
41. Duan Y, et al. (2003) A point-charge force field for molecular mechanics simulations of proteins based on condensed-phase quantum mechanical calculations. *J Comput Chem* 24:1999–2012.
42. Wang JM, Wang W, Kollman PA, Case DA (2006) Automatic atom type and bond type perception in molecular mechanical calculations. *J Mol Graphics Modell* 25:247–260.
43. Wang J, et al. (2004) Development and testing of a general Amber force field. *J Comput Chem* 25:1157–1174.